Solid State Science and Technology, Vol. 32, No. 2 (2024) 135-142
https://doi.org/10.66514/ssst32-2-135-142

Electrical Performance of NiO-CeO_2 Catalysts Layer for Anode-Supported Proton Ceramic Fuel Cells

Nur Farahin Yusoff[1], Zadariana Jamil[1,], Nafisah Osman[2], Nigel Brandon[3]*

[1]School of Civil Engineering, College of Engineering, Universiti Teknologi MARA 40450 Shah Alam, Selangor, Malaysia

[2]Faculty of Applied Sciences, Universiti Teknologi MARA, 02600 Arau, Perlis Malaysia

[3]Imperial College London, South Kensington Campus, London SW7 2AZ United Kingdom

**Corresponding author; email: zadariana@uitm.edu.my*

Received: 23 August 2024 / Accepted: 26 November 2024

ABSTRACT

Current research on PCFCs focuses mostly on the manufacturing of novel cell component materials, including the electrolyte, anode, and cathode, for a variety of cell geometries. It has been demonstrated that the microstructure of the electrodes has a significant impact on the cell performance; consequently, establishing the cell manufacturing technology is crucial for realizing the appropriate electrode microstructure and for creating new technologies to improve the performance of the electrodes. Recently, an anode catalyst layer (ACL) has been employed on the anode surface to improve fuel cell performance. This work reports on the electrical performance of NiO-CeO_2 catalysts layered onto NiO-BCZY (BCZY = $BaCe_{0.54}Zr_{0.36}Y_{0.1}O_{2.95}$) anode-supported proton ceramic fuel cell (PCFC) as CeO_2 has been reported to be a good promoter for PCFC and a good catalyst for hydrocarbon reforming reactions. The NiO-CeO_2 catalysts were incorporated onto the NiO-BCZY anode by spin-coating technique. The anode-supported NiO-BCZY|BCZY|LSCF (LSCF = $La_{0.6}Sr_{0.4}Co_{0.2}Fe_{0.8}O_{3-\alpha}$) button cells were fabricated using sol-gel, dry-pressing and spin-coating methods. The electrical performance of NiO-CeO_2/NiO-BCZY|BCZY|LSCF cell was analyzed in a hydrogen environment at a temperature of 800 °C using the electrochemical impedance spectroscopy (EIS) technique. The microstructure of the fabricated NiO-CeO_2/NiO-BCZY|BCZY|LSCF was characterized using scanning electron microscopy (SEM). The electrical performance of the NiO-CeO_2/NiO-BCZY|BCZY|LSCF shows ohmic and polarization resistance of 19.00 Ω cm^2 and 2.97 Ω cm^2, respectively. The ohmic resistance measured is considerably high due to lower electrolyte density and the delamination of catalyst at the catalyst-anode layer during the testing. SEM analysis indicates less dense BCZY electrolyte thin film with average pore size and porosity distribution of ~5.115 μm and 5.427%, respectively.

Keywords: Electrical Performance; NiO-CeO_2; Proton Ceramic Fuel Cell; NiO-BCZY; Anode-Supported.

INTRODUCTION

Fuel cells are effective power-generating systems that able to convert chemical energy into electricity electrochemically with little noise and pollution emission. They are anticipated to be utilized as portable and smaller power-producing devices as their scale drawbacks are minimal [1]. Among other fuel cell systems, solid oxide fuel cells (HT-SOFCs) demonstrate various dominance, including high fuel flexibility compared to other low-temperature fuel cells. The high working temperature, however, require the use of costly materials for cell components, a lengthy start-up phase, and a significant amount of energy input to heat the fuel cell to the working temperature, all of which hinder the SOFC commercialization and applications. Significant efforts have been made in the recent decades to develop proton-conducting SOFCs or proton ceramic fuel cells (PCFCs) that could work at lower intermediate temperatures and display a higher electromotive force (EMF) [2-6]. This advancement enables the use of less expensive connection materials and more reliable sealing, as well as improved control of electrode sintering or electrode-electrolyte interactions, hence increasing the operational lifetime of SOFCs [7-9].

NiO-BCZY anode supported PCFCs using BCZY electrolyte film are still being developed by the researchers because of their advantages of low cost and easy manufacturability. Furthermore, nickel oxide is the most efficient of the metal oxide sintering additives, exhibiting both good electrical conductivity and excellent catalytic activity of hydrogen oxidation and methane steam reforming [10,11]. Commonly, the NiO-BCZY anode is prepared by uniaxial pressing while the BCZY electrolyte is fabricated by spin-coating or screen-printing and the electrolyte/anode composite is co-fired above 1450 ºC [12]. A high Ni concentration in the standard NiO-BCZY anode, on the other hand, quickly causing cracks or warps of the NiO-BCZY|BCZY composite during co-firing due to the differences in thermal expansion coefficients and nickel agglomeration at high temperatures [13]. Thus, reducing the nickel content in the anode is recommended. To counter this phenomenon, Li et al. [14] who studied CeO_2-promoted catalyst reported that the addition of CeO_2 into monometallic nickel of $Ni/Al_2O_3–ZrO_2$ enhances the dispersion of Ni particles on the surface of catalyst and increases the nickel catalyst stability. Ahmed et al. [15] also found that CeO_2 has a significant impact on the activity and stability of the Ni/CeO_2-Al_2O_3 electrode, which also closely related with the nickel particles size and the structure of the catalyst.

Considering the commercialization purposes, the PCFC cells must also be flexible to hydrogen-rich fuels for robust applications. Changing pure hydrogen to hydrogen-rich fuels such as methane will drop the button cell performance, which mainly contributes to problems at the anode component. Although Ni-based anodes can reform CH_4 to H_2 and generate electricity in both wet methane reforming (WMR) and dry methane reforming (DMR) conditions, the carbon deposition, chemical instability of the anode and low conversion ratio in these atmospheres are critical challenges for this technology. Nickel catalysts were found to deactivate and degrade the PCFC (NiO-BCZY|BCZY|LSCF) performance as carbon deposited on the catalyst layer when the PCFC is fueled with dry methane, thus limiting triple phase boundary (TPB) sites. It has been reported that Ni catalysts with CeO_2 promoters can minimize the chemical interaction between nickel and support, increase nickel's reducibility and dispersion, and reduce coking [14,15]. The increased basicity of the supports and the highly reactive carbon species generated during the reaction are thought to inhibit carbon deposition [14].

In this preliminary work, we investigated the electrical performance of a modified button cell of NiO-BCZY|BCZY|LSCF with NiO-CeO_2 incorporated onto the anode,

which acts as a catalyst layer, in hydrogen atmosphere. The addition of NiO-CeO_2 was expected to improve the metallic dispersion, limit particle agglomeration, enhance the metal-support interactions, thus, increase the anode performance [14]. The microstructure analysis of the cell is confirmed through SEM and EIS techniques. This modified cell will later be used in the methane-fed fuel in our future study.

MATERIALS AND METHODS

Materials

The 20.0 wt.% NiO-CeO_2 catalyst was prepared by using nickel (II) nitrate, $Ni(NO_3)_2 \cdot 6H_2O$ (Sigma-Aldrich No. 13478-00-7) and cerium (III) nitrate, $Ce(NO_3)_3 \cdot 6H_2O$ (Sigma-Aldrich CAS No. 10294-41-4) with the aid of citric acid (Sigma-Aldrich, CAS No. 77-92-9) as binding ligands. The reagents, chemicals and processing routes that were used in the synthesis of NiO-BCZY composite anode, BCZY electrolyte powder, and LSCF cathode powder were explained in [11].

Powder synthesis of NiO-CeO_2 catalyst and NiO-BCZY|BCZY|LSCF cell

The NiO-BCZY anode, BCZY electrolyte, and LSCF cathode powder were initially prepared using a sol-gel technique previously described by Senari et al. [11]. The NiO-CeO_2 anode catalysts layer was prepared by dissolving 9.5820 g nickel (II) nitrate and 19.5390 g cerium (III) nitrate into 75 mL of deionized water. The mixture was then mixed with 16.7 vol% citric acid solution and stirred continuously at room temperature for 1 h. The mixed solution was continuously stirred and dried at 80 ºC using hot plate stirrer until a homogeneous gel obtained. The gel was dried further at 85 ºC in a drying oven (Venticell) for 12 h to form green powder. Next, this powder sample was ground using agate mortar and followed by roll-milling. Finally, the powder sample was calcined at 600 ºC for 5 h with a temperature increment rate of 10 ºC/min to produce 20 wt.% NiO-CeO_2 catalyst powder and then used for modified NiO-CeO_2/NiO-BCZY|BCZY|LSCF cell fabrication.

Fabrication of NiO-CeO_2/NiO-BCZYlBCZYlLSCF button cell

The NiO-CeO_2/NiO-BCZY|BCZY|LSCF button cell was fabricated using several steps. Firstly, the NiO-BCZY composite anode powder was weighed and uniaxially pressed at 9 tons for 7 min using a hydraulic press (Specac) coupled with a pellet die to obtain an anode pellet with a 25 mm diameter. Then, the BCZY electrolyte slurry was layered onto the anode pellet three times (three layers) using spin coating technique (2000 rpm for 30 seconds/layer) to form no across-layer pores. After every layer, the anode pellet-electrolyte thin film was dried in the oven at 100 °C for 10 min. The complete anode pellet-electrolyte thin film was then sintered at 1450 °C for 6 h in the air to attain sufficient mechanical rigidity. Next, the NiO-CeO_2 slurry was spin-coated on the surface of the anode pellet followed by LSCF thin film on the BCZY electrolyte. The complete NiO-CeO_2/NiO-BCZY|BCZY|LSCF single cells were sintered via a two-step sintering process of 600 °C (1 h), and then 950 °C (3 h). To conduct EIS testing, the button cell was pasted with platinum on both sites as the current collector and sintered for the last time at 900 °C for 1 h.

SEM and EIS analysis of the NiO-CeO_2/NiO-BCZY|BCZY|LSCF

The cross-section of NiO-CeO_2/NiO-BCZY|BCZY|LSCF was characterized using SEM analysis, Phenom XL Benchtop SEM (10 kV) assisted by a personal computer. The electrodes porosity (anode and cathode), delamination, cracks, and faults that may arise in the electrolyte thin film were also investigated.

The electrochemical performance of NiO-CeO_2/NiO-BCZY|BCZY|LSCF was measured using the EIS technique (Solartron S1 1260) under open circuit voltage (OCV) and Z-plot software. The measurement was performed at 800 °C where the hydrogen gas flow rate was set to be approximately 90 mL/min with the frequency range of 10^{-3} to 10^{6} Hz in a self-designed fuel cell test station. The impedance data acquired from the impedance testing were fitted using an equivalent circuit model and analyzed using ZMANTM 2.2 f3 (ZIVE LAB) software.

RESULTS AND DISCUSSION

SEM analyses of the button cell after EIS measurement

Figure 1 shows the cross-sectional microstructure of the anode-supported button cell of the (a) NiO-CeO_2/NiO-BCZY site and the (b) NiO-BCZY|BCZY|LSCF site. From Figure 1(b), there was no delamination observed between the anode-electrolyte and electrolyte-cathode layers. After EIS measurement, there were also no cross-layer pores and cracks observed at the anode-electrolyte layer. However, there was delamination found at the catalyst-anode layer in Figure 1(a) where some parts of the catalysts layer delaminated during the EIS analysis. This might be due to the lower sintering temperature of the layer which is 900 °C compared to the temperature suggested by Jamil et al. which is 1300 °C [16]. The thickness of the BCZY thin film measured was approximately 136 µm since the BCZY slurry was pasted three layers on the anode however it was thicker than the optimum thickness (10-20 µm) for an electrolyte thin film as reported by Bi et al. [17] in reducing the ohmic loss which enables lower operating temperature and higher performance.

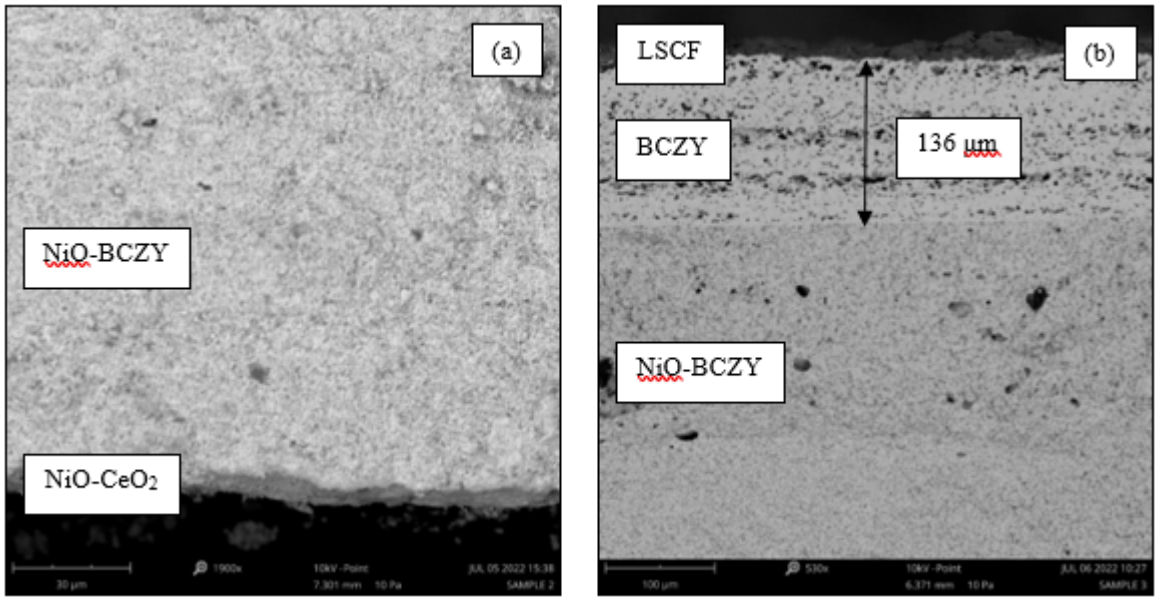

Figure 1. Cross-sectional microstructure of the completed button cell (a) NiO-CeO_2/NiO-BCZY site; (b) NiO-BCZY|BCZY|LSCF site

The pore size of the electrolyte was analyzed using SEM images at a magnification of 590× (Figure 2). The pores size in BCZY electrolyte measured using ImageJ software was found to be approximately 5.115 µm having lower density than reported by Lee et al. [18], where the pores in this study were found to be larger having

more open pores. The porosity distribution of the electrolyte measured using SEM images was also analyzed using ImageJ software. It was found that the BCZY electrolyte has higher porosity (5.427%) which is not within the range of desired porosity (less than 5%) for PCFC electrolyte [19]. From the analysis, the BCZY electrolyte thin film was found to be not well densified, and many close pores were observed which may be due to the method used to prepare the BCZY slurry. This condition of electrolyte may affect the electrical performance of the NiO-CeO_2/NiO-BCZY|BCZY|LSCF button cell as a dense electrolyte is important for PCFCs to ensure excellent gas-tightness thus, improves the cell performance [20].

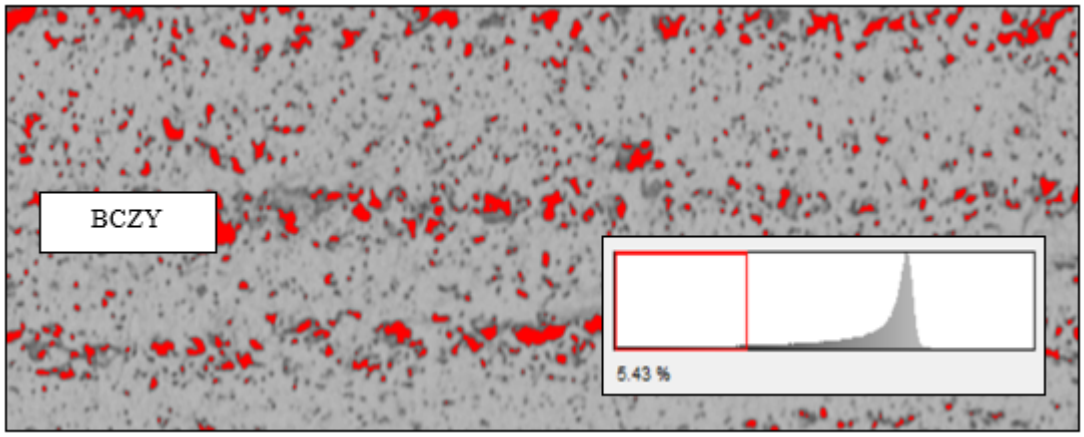

Figure 2. SEM cross-section image and porosity analysis of BCZY electrolyte at a magnification of 590× using ImageJ software

EIS analysis

Figure 3 shows a few resistances that were measured from the impedance spectra, which are ohmic resistance (R_o), polarization resistance (R_p), and total resistance (R_t). The R_o demonstrates electrolyte resistance while R_p indicates electrode resistance. The ohmic response is represented by the high-frequency intercept with the real axis, while the difference between the high- and low-frequency intercepts indicates the interfacial response or R_p [21]. The addition of both R_o and R_p will give the value for the total resistance of the NiO-CeO_2/NiO-BCZY|BCZY|LSCF anode-supported button cell. The total polarization of a full cell is the total of several processes related to ohmic losses, anode diffusion, and cathode polarization, which were attributed to the cell electronic/ionic charge transfers between 10^{-3} to 10^{6} Hz [22]. In addition, non-charge transfer activities were associated with the diffusion of H_2/O_2 across the electrode pores in the low-frequency area of 10^{-3} Hz. The abovementioned resistance statistics can be derived through a fitting technique with an equivalent electrical circuit model shown in the inset of Figure 3. The amplitude voltage supplied used during EIS analysis was 5 mV.

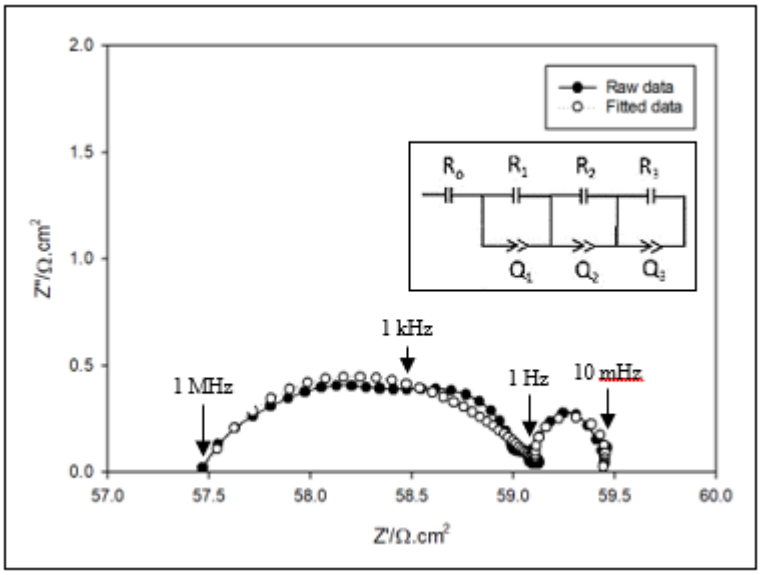

Figure 3. Impedance spectra of NiO-CeO_2/NiO-BCZY|BCZY|LSCF measured at 800 °C

The measurements of the impedance of NiO-CeO_2/NiO-BCZY|BCZY|LSCF cell were conducted under fuel cell conditions at a temperature of 800 °C in a hydrogen atmosphere (10% H_2). The impedance spectra showed that at 800 °C the arcs were formed, with the first and the second arc can easily be distinguished. The R_p was achieved at 2.97 Ω cm^2, showing improvement from the polarization resistance obtained in our previous study (7.77 Ω cm^2) on a NiO-BCZY|BCZY|LSCF single cell analyzed at 700 °C in hydrogen atmosphere [11]. The R_o measured for the cell was 19.00 Ωcm^2, deviated to the previous study done by Senari et al. [11] which is 9.57 Ω cm^2 at 700 °C. As ohmic resistance depends on the conductivity of the electrolyte and the geometry of the electrode, the higher ohmic resistance measured may be assigned to the delamination of the catalysts layer that affects the reaction layer and hydrogen oxidation charge transfer kinetics at the catalyst and anode layers. The high ohmic resistance may also be attributed from the lower density and thicker electrolyte layer as observed during SEM analysis. Customizing the anode microstructure will result in increased catalytic activity for the reaction of H_2 oxidation and superior transfer of H_2 gas, as well as improved adhesion between the anode and electrolyte, which contributes to the decrease of the polarization and ohmic resistances [21,23,24].

CONCLUSIONS

A NiO-CeO_2/NiO-BCZY|BCZY|LSCF button cell was synthesized and fabricated using sol-gel and spin-coating methods. The electrochemical performance of the cell was tested in H_2 at 800 °C with a flow rate of 90 mL/min. The ohmic and polarization resistances of the cell were achieved at 19.00 Ω cm^2 and 2.97 Ω cm^2, respectively. The higher ohmic values may be closely related to the delamination of the catalyst layer that has affected the reaction layer and H_2 oxidation charge transfer kinetics at the anode and catalyst layer. The study on modifying the sintering temperature of the catalyst-anode layer will be considered in our future work to improve the contact between the catalyst and anode. In addition, the high ohmic resistance of the cell might also be due to the low density and thicker electrolyte layer. Whilst the cell achieved higher ohmic values, some modification of the fabrication and processing techniques will reduce the delamination and low

electrolyte density issues and offer an improvement in the electrochemical performance of the NiO-CeO_2/NiO-BCZY|BCZY|LSCF cells.

ACKNOWLEDGMENTS

This work was financially supported by the Universiti Teknologi MARA (UiTM) through the Global Research Reputation (GRR), 600-RMC 5/3/GRR (006/2020) grant and the Research Incentive Grant (GIP), 600-RMC/GIP 5/3 (149/2021). The authors also thank UiTM Shah Alam and UiTM Perlis branch for the facilities and support provided throughout the research.

REFERENCES

[1] K. Sasaki, I. Takahashi, K. Kuramoto, K. Shin-mura (2022). A high-performance Ni-CeO_2/Ni/Ni-Y_2O_3·ZrO_2 three-layer anode for direct iso-octane feeding of solid oxide fuel cells, *R. Soc. Open Sci.* **9**(7), 220227

[2] S. Hossain, A.M. Abdalla, J.H. Zaini, C.D. Savaniu, J.T.S. Irvine, A.K. Azad (2017). Highly dense and novel proton conducting materials for SOFC electrolyte, *International Journal of Hydrogen Energy* **42**(44), 27308.

[3] G. Chen, Y. Luo, W. Sun, H. Liu, Y. Ding, Y. Li, S. Geng, K. Yu, G. Liu (2018). Electrochemical performance of a new structured low temperature SOFC with BZY electrolyte, *International Journal of Hydrogen Energy* **43**(28), 12765.

[4] E. Fabbri, A. D'Epifanio, E. di Bartolomeo, S. Licoccia, E. Traversa (2008). Tailoring the chemical stability of $Ba(Ce_{0.8-x}Zr_x)Y_{0.2}O_{3-\delta}$ protonic conductors for intermediate temperature solid oxide fuel cells (IT-SOFCs), *Solid State Ion*. **179**(15–16), 558.

[5] M.A. Azimova, S. McIntosh (2010). Properties and performance of anode-supported proton-conducting $BaCe_{0.48}Zr_{0.4}Yb0.1Co_{0.02}O_{3-\delta}$ solid oxide fuel cells, *J. Electrochem. Soc.* **157**(10), B1397.

[6] G.C. Mather, M.S. Islam (2005). Defect and dopant properties of the $SrCeO_3$-based proton conductor, *Chemistry of Materials* **17**(7), 1736.

[7] C.J. Tseng, J.K. Chang, I.M. Hung, K.R. Lee, S.W. Lee (2014). $BaZr_{0.2}Ce_{0.8-x}Y_xO_{3-\delta}$ solid oxide fuel cell electrolyte synthesized by sol-gel combined with composition-exchange method, *International Journal of Hydrogen Energy* **39**(26), 14434.

[8] J.W. Fergus (2006). Electrolytes for solid oxide fuel cells, *Journal of Power Sources* **162**(1), 30.

[9] K.R. Lee, C.J. Tseng, J.K. Chang, I.M. Hung, J.C. Lin, S.W. Lee (2013). Strontium doping effect on phase homogeneity and conductivity of $Ba_{1-x}Sr_xCe_{0.6}Zr_{0.2}Y_{0.2}O_{3-\delta}$ proton-conducting oxides, *International Journal of Hydrogen Energy* **38**(25), 11097.

[10] K. Thabet, A. le Gal La Salle, E. Quarez, O. Joubert (2020). Protonic-based ceramics for fuel cells and electrolyzers. Solid Oxide-Based Electrochemical Devices: Advances, *Smart Materials and Future Energy Applications.* Elsevier, 91–122.

[11] S.M. Senari, N. Osman, A.M.M. Jani (2018). Impedance study on NiO-$BaCe_{0.54}Zr_{0.36}Y_{0.1}O_{2.95}$ composite anode for proton-conducting fuel cell, *Journal of Physics: Conference Series* **1083**, 012026.

[12] Z. Zhu, E. Guo, Z. Wei, H. Wang (2018). Tailoring $Ba_3Ca_{1.18}Nb_{1.82}O_{9-\delta}$ with NiO as electrolyte for proton-conducting solid oxide fuel cells, *Journal of Power Sources* **373**, 132.

[13] J. Qiao, K. Sun, N. Zhang, B. Sun, J. Kong, D. Zhou (2007). Ni/YSZ and Ni-CeO2/YSZ anodes prepared by impregnation for solid oxide fuel cells, *Journal Power Sources* **169**(2), 253

[14] H. Li, H. Xu, J. Wang (2011). Methane reforming with CO_2 to syngas over CeO_2-promoted Ni/Al_2O_3-ZrO_2 catalysts prepared via a direct sol-gel process, *Journal of Natural Gas Chemistry* **20**(1), 1.

[15] W. Ahmed, A.E. Awadallah, A.A. Aboul-Enein (2016). Ni/CeO_2–Al_2O_3 catalysts for methane thermo-catalytic decomposition to CO_x-free H_2 production. *International Journal of Hydrogen Energy* **41**(41), 18484.

[16] Z. Jamil, E. Ruiz-Trejo, P. Boldrin, N. P. Brandon (2016). Anode fabrication for solid oxide fuel cells: electroless and electrodeposition of nickel and silver into doped ceria scaffolds, *International Journal of Hydrogen Energy* **41**(22), 9627.

[17] L. Bi, E. Fabbri, Z. Sun, E. Traversa (2011). $BaZr_{0.8}Y_{0.2}O_{3-\delta}$-NiO composite anodic powders for proton-conducting SOFCs prepared by a combustion method, *J. Electrochem. Soc.* **158**(7), B797.

[18] K.R. Lee, C.J. Tseng, S.C. Jang, J.C. Lin, K.W. Wang, J.K. Chang, T.C. Chen, S.W. Lee (2019). Fabrication of anode-supported thin BCZY electrolyte protonic fuel cells using NiO sintering aid, *Int. J. Hydrogen Energy* **44**(42), 23784.

[19] M. Rafique, N. Safdar, M. Irshad, M. Usman, M. Akhtar, M. W. Saleem, M. M. Abbas, A. Ashour and M. E. Soudagar (2022). Influence of low sintering temperature on $BaCe_{0.2}Zr_{0.6}Y_{0.2}O_{3-\delta}$ IT-SOFC perovskite electrolyte synthesized by co-precipitation method, *Materials* **15**(10), 3585.

[20] M. Ahsan, M. Irshad, P.F. Fu, K. Siraj, R. Raza, F. Javed (2020). The effect of calcination temperature on the properties of Ni-SDC cermet anode, *Ceram. Int*. **46**(3), 2780.

[21] T. Yamaguchi, H. Sumi, K. Hamamoto, T. Suzuki, Y. Fujishiro, J.D. Carter, S.A. Barnett (2014). Effect of nanostructured anode functional layer thickness on the solid-oxide fuel cell performance in the intermediate temperature, *Int. J. Hydrogen Energy* **39**(34), 19731.

[22] R. Barfod, M. Mogensen, T. Klemenso, A. Hagen, Y.-L. Liu, P. Vang Hendriksen (2007). Detailed characterization of anode-supported SOFCs by impedance spectroscopy, *Journal Electrochem. Soc*. **154**(4), B371.

[23] K.R. Lee, C.J. Tseng, J.K. Chang, K.W. Wang, Y.S. Huang, T.C. Chou, L.D. Tsai, S.W. Lee (2019). Nano-fibrous $SrCe_{0\cdot8}Y_{0\cdot2}O_{3-\delta}$-Ni anode functional layer for proton-conducting solid oxide fuel cells. *Journal Power Sources* **436,** 226863.

[24] S. He, H. Dai, G. Cai, H. Chen, L. Guo (2015). Optimization of $La_{0.75}Sr_{0.25}Cr_{0.5}Mn_{0.5}O_{3-\delta}$-$Ce_{0.8}Sm_{0.2}O_{1.9}$ compositionally graded anode functional layer, *Electrochim Acta* **152**, 155.